

Tropical Atlantic sea surface temperature variability and its relation to El Niño-Southern Oscillation

David B. Enfield and Dennis A. Mayer

Atlantic Oceanographic and Meteorological Laboratory, NOAA, Miami, Florida

Abstract. Past analyses of tropical Atlantic sea surface temperature variability have suggested a dipole behavior between the northern and southern tropics, across the Intertropical Convergence Zone (ITCZ). By analyzing an improved 43-year (1950-1992) record of SST [Smith *et al.*, 1996] and other data derived from the Comprehensive Ocean-Atmosphere Data Set (COADS), it is shown that the regions north and south of the ITCZ are statistically independent of each other at the seasonal to interannual timescales dominating the data, confirming the conclusions of Houghton and Tourre [1992]. Some dipole behavior does develop weakly during the boreal spring season, when there is a tendency for SST anomaly west of Angola to be opposite of that in the tropical North Atlantic. It is further shown that tropical Atlantic SST variability is correlated with Pacific El Niño-Southern Oscillation (ENSO) variability in several regions. The major region affected is the North Atlantic area of NE trades west of 40°W along 10°N - 20°N and extending into the Caribbean. There, about 50-80% of the anomalous SST variability is associated with the Pacific ENSO, with Atlantic warmings occurring 4-5 months after the mature phases of Pacific warm events. An analysis of local surface flux fields derived from COADS data shows that the ENSO-related Atlantic warmings occur as a result of reductions in the surface NE trade wind speeds, which in turn reduce latent and sensible heat losses over the region in question, as well as cooling due to entrainment. This ENSO connection is best developed during the boreal spring following the most frequent season of maximum ENSO anomalies in the Pacific. A region of secondary covariability with ENSO occurs along the northern edge of the mean ITCZ position and appears to be associated with northward migrations of the ITCZ when the North Atlantic warmings occur. Although easterly winds are intensified in the western equatorial Atlantic in response to Pacific warm events, they do not produce strong local changes in SST. Contrary to expectations from studies based on equatorial dynamics, these teleconnected wind anomalies do not give rise to significant correlations of SST in the Gulf of Guinea with the Pacific ENSO. As the teleconnection sequence matures, strong SE trades at low southern latitudes follow the development of the North Atlantic SST anomaly and precede by several months the appearance of weak negative SST anomalies off Angola and stronger positive anomalies extending eastward from southern Brazil along 15°-30°S.

1. Introduction

As a result of the Tropical Ocean—Global Atmosphere (TOGA) program (1985-1994), progress has been made in modeling the coupled ocean-atmosphere system in the Pacific known as El Niño - Southern Oscillation (ENSO). It is generally believed that various kinds of models have skill in predicting the sea surface temperature (SST) increases in the tropical Pacific, associated with warm phases of the ENSO cycle, from several months to a year in advance [Barnston *et al.*, 1994]. Empirical studies, such as Ropelewski and Halpert [1987], have established teleconnective relationships between the Pacific ENSO and land climate variability around the globe. New programs, such as the Global Ocean-Atmosphere-Land Studies (GOALS), are predicated on the notion that short-term (seasonal to interannual) climate variability is also influenced by the interactions between the troposphere and other regions of the world ocean, especially the Indian and tropical Atlantic

basins, and that additional predictability can be achieved by incorporating those oceans into the model schemes. Much less is known about the additional predictability that other ocean areas can provide, and even less is known about how other oceans interact with the strong ENSO signal in the tropical Pacific.

Many empirical studies have already demonstrated the relationship of various regional climates to SST variability in the Atlantic [e.g., Moura and Shukla, 1981; Folland *et al.*, 1986]. These studies have shown that the climates of northeast (NE) Brazil and northwest (NW) Africa are especially sensitive to a meridional seesaw behavior between the SST anomalies (SSTA) north and south of the equator. Some multivariate analyses of SST [e.g., Weare, 1977; Hastenrath, 1978] suggest that a natural tendency exists for the tropical Atlantic SST to fluctuate antisymmetrically like a dipole. Others [e.g., Houghton and Tourre, 1992] show that the two regions separate (under rotation) into modes where the explained variability is heavily weighted on one side of the equator or the other. This suggests that a true dipole does not really exist. Hence, while the climate sensitivity approach has bolstered a widely held impression that the tropical Atlantic is dipolar, studies that consider SST alone have yielded mixed results.

Understanding the interbasin effects of ENSO is also important if the true (as opposed to apparent) predictability of other

This paper is not subject to U.S. copyright. Published in 1997 by the American Geophysical Union.

Paper number 96JC03296.

basins is to be estimated. For example, if SST variabilities in the Pacific and the Atlantic are not totally independent of each other and both are related to certain regional rainfall patterns, to what extent does each ocean have a truly causative relationship with rainfall? Moreover, the predictive performance of global coupled models now under development can be enhanced by incorporating improvements based on empirical knowledge of the processes linking the basins (which the models must successfully reproduce). The presence of Pacific ENSO variability in the Atlantic sector, and/or internal variability that is "ENSO-like", has been explored by several studies. *Hastenrath et al.* [1987] find correlations of the Southern Oscillation Index (SOI) with various ship-reported variables in the Atlantic (1935-1983, 30°S-30°N) and with terrestrial rainfall. Their results confirm and expand upon the findings of *Covey and Hastenrath* [1978]. For positive phases of the SOI during the boreal spring (April-May), the most salient and significant features of contemporaneous (zero lag) correlation structures include (1) SST reduction and sea level pressure (SLP) increase in the tropical North Atlantic, (2) more northerly meridional winds (V , 15°S-15°N) and a southward shift of the Intertropical Convergence Zone (ITCZ), and (3) an increase of rainy season precipitation in NE Brazil. Secondary features of less significance include (4) warmer SST in the tropical South Atlantic and (5) more easterly zonal wind (U) in the region north of the ITCZ and more westerly zonal wind in the region south of the ITCZ. During the boreal summer (July-August) the relationships appear to be weaker (SST, V), or reversed (SLP, ITCZ, U) and NW African rainfall increases. The Atlantic sector interactions implied by these relationships are mutually consistent with the sense expected from other studies of Atlantic variability without regard to ENSO [e.g., *Hastenrath et al.*, 1984; *Moura and Shukla*, 1981].

Modeling results that successfully reproduce the *Hastenrath et al.* [1987] relationships are found in the the Oregon State University (OSU) coupled model study of *Hameed et al.* [1993]. This is particularly true of the region north of the ITCZ, while relationships involving the South Atlantic appear weaker or even contradictory. The most interesting additional information emerging from their study is that during ENSO warm phases, or low SOI, the subtropical high pressure system and associated trade circulation are weakened in the tropical North Atlantic and strengthened in the tropical South Atlantic. These conditions are accompanied by significant ENSO-associated SST increases in the NE trades region, which also extend through most of the upper ocean thermal structure, and by the expected rainfall decreases in northern South America. The authors conclude that the ENSO signal enters the North Atlantic through the atmosphere, in association with a weakened Walker Circulation. This conclusion is also consistent with the teleconnections between the Pacific ENSO variability and the midtropospheric North Atlantic sector [*Wallace et al.*, 1990]. The exact nature of the air-sea coupling responsible for the warming is not specified in any of these studies, but they are consistent in that Atlantic-Pacific relationships involving Atlantic SST north of the ITCZ appear to be stronger than those involving areas near and south of the ITCZ.

Two modeling studies deserve mention. Using a coupled model with delayed-oscillator dynamics, *Zebiak* [1993] finds that ENSO-like variability occurs in the equatorial Atlantic, but it is statistically uncorrelated with the Pacific ENSO. However, because the simulation involves only near-equatorial dynamics, the study says nothing about whether this mechanism can account for the Atlantic correlations with the Pacific ENSO found by *Hastenrath et al.* [1987] and *Hameed et al.* [1993]. In coupled and uncoupled simulations using global models, *Latif and Barnett* [1995] find easterly wind anomalies off NE Brazil and cooler SSTs in the Gulf of Guinea, in association with Pacific ENSO warmings. We note that these results are mechanis-

tically consistent with an atmospheric teleconnection from a warm Pacific to easterly wind anomalies in the eastern equatorial Atlantic, followed by a dynamical cooling response in the Gulf of Guinea as shown by *Zebiak* [1993]. It is noteworthy, however, that none of the observed relationships at extra-equatorial latitudes [*Hastenrath et al.*, 1987; *Hameed et al.*, 1993] are reproduced by *Latif and Barnett* [1995] nor by *Zebiak* [1993].

Considering the ambiguities and incomplete description of the Atlantic ENSO connections and in view of emerging efforts to relate western hemisphere climate to Atlantic as well as Pacific SST variability, it seems especially appropriate at this time to more completely explore the spatial and seasonal nature of the ENSO connections and to specify the mechanisms by which the troposphere forces the mixed layer temperature. This study uses somewhat different data sets for a different and longer time period than in the studies cited above and finds important areas of consistency, especially with *Hastenrath et al.* [1987] and *Hameed et al.* [1993], but also significant areas of departure, mainly in the South Atlantic and also with respect to the studies of *Latif and Barnett* [1995] and *Zebiak* [1993] outside of the equatorial strip. In general, where previous results are robust, we find agreement, where they are weak, we find differences. More importantly, the probable ENSO-associated forcing mechanisms are identified. After explaining the data sets and methods used (section 2), we describe the structure of the Atlantic SST variability and document the correlations associated with Pacific variability (section 3), consider how the relationships vary by season (section 4), and examine the possible causes (section 5). In section 6 we discuss the results in relation to previous findings.

2. Data and Methods

The data used in this study are extracted or derived from the Comprehensive Ocean-Atmosphere Data Set (COADS) [*Woodruff et al.*, 1987] compiled from ship reports. The sea surface temperatures are a reconstructed version of the COADS SST data prepared by *Smith et al.* [1996]. Both the COADS data and the *Smith et al.* [1996] SSTs are averaged by month and 2° squares for the Pacific and Atlantic. We have selected 30°S-30°N and from 1950 through 1992 (43 years) as the space-time domain for our analysis. The choice of time period is based on the coverage of the *Smith et al.* [1996] SST reconstruction and is also influenced by the deterioration of COADS data coverage prior to the 1950s. Although data density is not uniform over the selected period, it seems to be adequate, especially north of about 10°S in the Atlantic.

For the most critical variable, SST, the *Smith et al.* [1996] data appear to have significant advantages over the original COADS. For COADS the signal-to-noise ratio is lower in the more poorly sampled regions, e.g., those having fewer than about five observations per month per 2° square. This is undoubtedly due to aliasing by fine spatial scale structures (e.g., eddies) and unresolved temporal variability (e.g., diurnal cycle). The lower signal-to-noise ratio can be readily seen by examining the distributions of local variance explained by low-order empirical orthogonal function (EOF) modes that filter out small-scale variability and noise. In poorly sampled regions such as the tropical Pacific (Figure 1a) these distributions show considerable "trackiness", that is, the variance explained is high in the vicinity of well-sampled ship routes and low in poorly sampled regions. Spatial interpolation by objective mapping does not improve this very much because individual maps have gaps much larger than the decorrelation scale over which signal variability can be interpolated effectively. In the *Smith et al.* [1996] reconstruction, gaps in the COADS data are

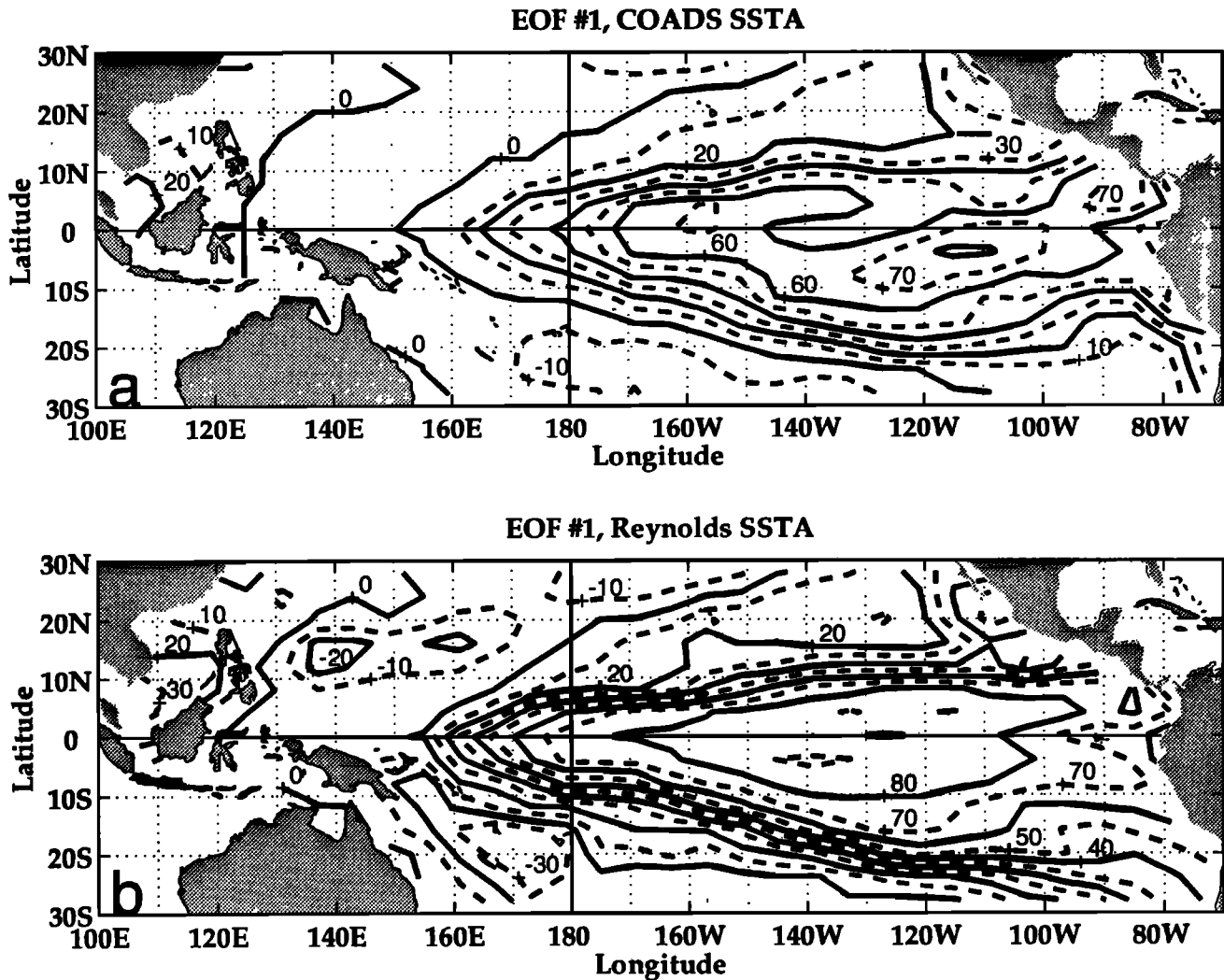


Figure 1. The dominant (first mode) empirical orthogonal function (EOF) pattern for 1950-1992 Pacific sea surface temperature departures (SSTA) according to (a) the Comprehensive Ocean-Atmosphere Data Set (COADS) and (b) *Smith et al.* [1996]. Contoured is the signed, squared correlation of the temporal expansion coefficients for the mode with the SSTA at each location. The values are expressed as the percent of local variance explained and are multiplied by the sign of the eigenvector values at the corresponding locations so that regions of opposite loading are distinguishable.

filled by fitting the available data, in the least squares sense, to an ensemble of the leading 24 EOF modes of well sampled and optimally analyzed SST from ships, satellites, and buoys, for the period 1982-1993. The first EOF of the 1950-1992 reconstruction shows a more plausible distribution of explained variance without the trackiness (Figure 1b). In well-sampled regions the reconstructed data retain the explained variance of the original data (Figure 1a), while in adjacent, poorly sampled regions the explained variance is brought up to reasonable values. The temporal expansion coefficients (not shown) of the EOF modes in Figure 1 are virtually identical.

The *Smith et al.* [1996] SST data for the Pacific and Atlantic and the non-SST COADS data for the Atlantic are processed into 3-month running mean (3MRM) maps of SST, vector wind components (U , V), wind speed (W), pseudostress components (WU , WV), and sea level pressure (SLP), for 1950-1992. The first and last maps for the *Smith et al.* [1996] SSTs are 2-month means for January-February 1950 and November-December 1992, respectively.

Prior to time averaging, temporal gaps of 1 to 6 months (in the non-SST data) are bridged with an autoregressive algorithm. The data are then averaged into 3MRM maps, where any bin having less than two nonmissing months is assigned a missing-data flag. Finally, the missing bins in each map are filled by an objective method that minimizes a cost function based on the data surrounding a gap [*Donoso et al.*, 1994]. This is done mainly for convenience in the subsequent calculation of derivative fields such as wind stress curl, surface wind divergence, etc.

To assess the impact of the gapfilling, we make the worst-case assumption that such filling deteriorates the large-scale structures in the data to no greater extent than leaving the gaps in the data. Numerical experiments were then run on two kinds of gapless data: the *Smith et al.* [1996] SST anomalies in the tropical Pacific and complete time series of rain gauge data over the continental United States (1950-1980). Rainfall is used here only as an expedient because complete series are available and its natural variability is notoriously noisy (as

compared with SST) and may be more representative than SST of the atmospheric variables in COADS. Gaps were repetitively introduced into the data (10 random trials each) at 5% increments of decimation. Their EOFs were recalculated and the resulting eigenvectors were compared by correlation with the original (control run) eigenvectors of the gapless data. For both types of data it was found that the large-scale structures of the data as represented by the first 15 modes remain highly correlated with the control run as long as the degree of decimation is 15% or less. The first few leading modes retain their integrity well beyond the 15% point, but correlations for the higher modes begin to deteriorate.

The only area where the gappiness of the (non-SST) Atlantic COADS data exceeds 15% is found off southern Brazil, south of 10°S and west of the Greenwich meridian, a region that does not greatly affect the conclusions of this paper. Only the gapless *Smith et al.* [1996] SST data are used in the Pacific where gap-filling procedures (like those described here) become more risky.

Following the above steps, the SST data are resummized from the original 2° grid into 4° latitude by 6° longitude bins. These coarse resolution data are used in most descriptive and statistical analyses, for convenience but also for consistency because the *Smith et al.* [1996] reconstruction of SST is essentially a method that filters out small-scale time-space variability in the data. The fine resolution grid is retained for the computation and analysis of derivative fields such as evaporative heat flux, wind stress curl, and wind divergence (section 5).

Subsequent analyses include computation of the annual cycles (averaged by calendar month over 43 years) and the departures from them (anomalies). EOFs are computed by calculating the singular value decomposition (SVD) of the unnormalized data array, which gives identical results to calculation of the eigenvectors of the covariance matrix but is numerically more stable. We have made extensive use of scalar and vector correlations of Atlantic data fields against temporal indices such as EOF expansion coefficients. The vector correlation involves computation of the time-domain covariance between two complex-valued sequences [Kundu, 1976]. Wherever appropriate, the means are removed from the data. Linear trends were subtracted only from the COADS wind-related data because the winds have a large increasing trend related to the transition from Beaufort estimates to anemometers [Cardone et al., 1990].

We estimate the significance values for correlations by the method of *Sciremammano* [1979], which accounts for serial correlation in the time series. The correlations corresponding to a particular significance level will vary according to the integral timescale as determined by the autocorrelation functions, even though the nominal degrees of freedom (length of time series) may not vary. Thus variables dependent on wind speed (e.g., evaporation rate) have shorter timescales, more effective degrees of freedom, and lower significance levels than those based on temperature (e.g., SST indices). On the other hand, correlations for variables averaged over large areas (e.g., SST indices) will have longer timescales, fewer effective degrees of freedom, and higher significance levels than for time series in the individual, component grid-box averages.

3. Atlantic SST Structures and Their Relationship to ENSO Variability

This section characterizes the relevant nonseasonal Pacific SST variability in the form of a single index, dominated by ENSO, as a reference for comparison with Atlantic variability. Comparison of the Pacific index with two similarly derived Atlantic SST indices gives a coarse idea of how the principal Atlantic SST structures are related to the Pacific ENSO variabil-

ity. Finally, fields of lagged cross correlation, between the gridded Atlantic data and the Pacific index, document in detail how the ENSO-related SSTA variability is distributed in the Atlantic. The relationships are first explored for all months without regard to season (this section) and then broken down seasonally to see where similarities and differences occur (sections 4 and 5).

3.1. An Index of Pacific SSTA Variability

The Pacific SST index, P_1 , is taken to be the normalized temporal expansion coefficients of the first EOF mode of the covariance matrix of SSTA in the Pacific. The P_1 index explains 52% of the total Pacific nonseasonal variance in the 3MRM data (30°S–30°N) and 75–90% of the local variance over a large portion of the $\pm 10^\circ$ region (Figure 1b). The spatial distribution of local variance explained is very much like the composite SSTA distribution found by *Rasmusson and Carpenter* [1982] for the mature phases of six historical El Niño events in the 1950s, 1960s, and 1970s. There is a maximum cross correlation of 0.97 at zero lag between the P_1 index and the average SSTA of the *Smith et al.* [1996] data over the region 6°S–6°N, 90°W–150°W. Hence the P_1 index is virtually identical with the NINO3 index (5°S–5°N, 90°W–150°W) frequently used in other studies, and it typifies equatorial Pacific SSTA variability that reaches its extreme values at the mature phases (cool or warm) of ENSO cycles.

3.2. Annual Variability in the Atlantic

Figure 2 shows the 43-year mean SST and wind (U , V) distributions in the Atlantic for the antipodal seasons centered on February and August. These are also the boreal winter-spring and summer-fall periods relevant to the rainy seasons in NE Brazil and NW Africa, respectively. Some of the subsequent analyses of anomalous variability can be referenced to these normals. The basic wind-SST relationship, which remains qualitatively the same all year long, is of surface winds in the tropics of both hemispheres crossing isotherms toward the warmest water, typically located in the Caribbean and below the low-level wind confluence that defines one aspect of the ITCZ. The NE and SE trades are strongest in February (warmest South Atlantic) and August (warmest North Atlantic), respectively, and the ITCZ is either close to the equator (February) or joins sub-Saharan Africa with northern South America along 9°–10°N (August). In both seasons, there is southerly flow from the eastern South Atlantic into NW Africa across the Gulf of Guinea, but this flow is stronger in August. Upwelling favorable winds affect the coast of NW Africa north of 12°N and the entire African coast between the equator and 30°S. The winds in both seasons flow from the Caribbean into the equatorial Pacific across Panama and Costa Rica, but the flow is much stronger in February. As will become apparent, anomalous large-scale thermal distributions in the Pacific (indexed by P_1) are associated with alterations of these wind features, which in turn force SST responses in the Atlantic.

3.3. Atlantic Departure Variability

The nonseasonal variability of Atlantic SST and winds can be described in terms of the dominant EOF modes of SSTA and the vector correlations of the COADS surface winds with those modes. The distributions of local variance explained by the first two Atlantic EOF modes are contoured in Figure 3, and the zero-lag vector correlations of the nonseasonal winds with the respective modal expansion coefficients are superimposed. So as to also show areas of anticorrelation within each mode, the signs from the eigenvector matrix are assigned to the corresponding elements of the explained variance matrix. The time

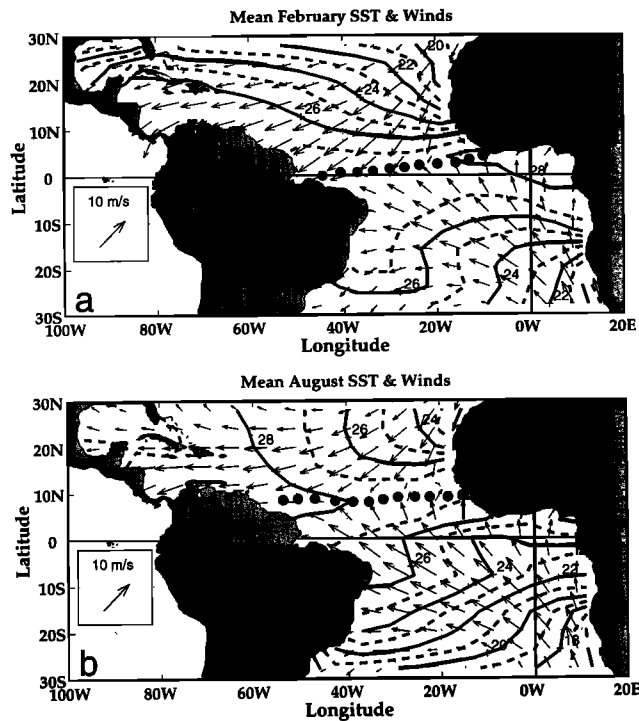


Figure 2. Patterns of climatological mean Atlantic SST and surface winds for (a) February and (b) August. The corresponding mean ITCZ positions, determined from the divergence of the surface winds, are shown as solid circles. The inset west of South America sets the scale for the vector field.

domain variability of the Atlantic modes and of the P_1 index to which they will be compared is shown in Figure 4. Because the first mode has negative eigenvector loadings in the region of high explained variance (Figure 3a), negative values of its temporal expansion coefficients (Figure 4, top) imply modal warming over the same region. The eigenvalue difference between these two modes is such that their sampling errors [North *et al.*, 1982] do not overlap [e.g., Houghton and Tourre, 1992]. Thus the modes are well separated and the decomposition is stable.

The two dominant modes of tropical Atlantic SSTA describe variability located south (A_1) and north (A_2) of the ITCZ within the trade wind regions and explain 32% and 21% of the total variability, respectively (Figure 3). Together they account for 53% of the total SSTA variance, while individually they explain 50-80% of the local variance in their respective regions. In both cases, the anomalous winds are directed toward the hemisphere dominated by modal warming. The only regions where the eigenvectors change sign are in two areas of the A_2 pattern (Figure 3b): one in the Gulf of Mexico, extending eastward past the Florida peninsula, and the other over a large region south of the equator. In both cases the amplitudes and explained local variance are very small. These will be discussed further in Sections 4, 5, and 6. In subsequent discussions we will refer to the areas of large explained variance, south and north of the ITCZ, as the A_1 and A_2 regions, respectively.

The A_1 and A_2 modes are necessarily uncorrelated at zero lag, but the correlation is also low and insignificant at all lags within ± 15 months of zero. Significant correlation exists at very large lags, however, consistent with indications from Mehta and Delworth [1995] and Huang *et al.* [1995] that a dipole relationship exists at decadal or greater timescales. Be-

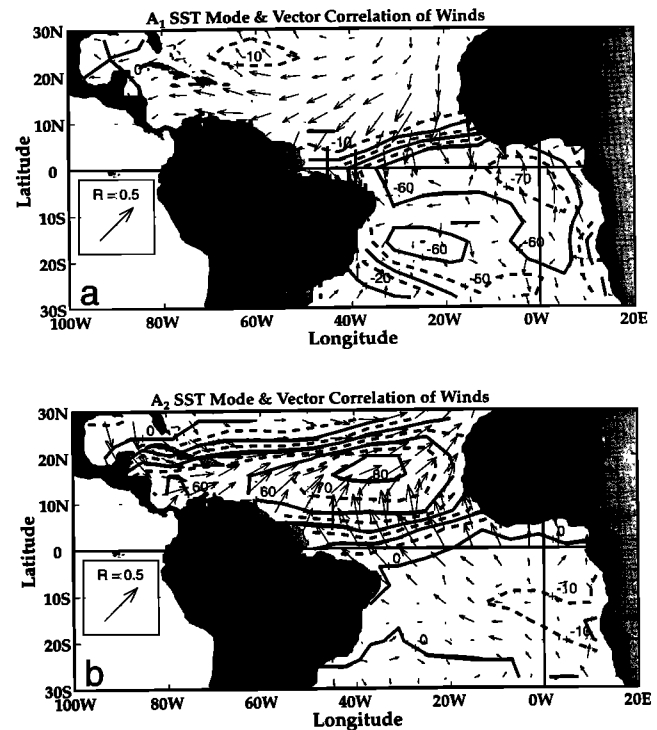


Figure 3. As in Figure 1, for (a) the first and (b) the second EOF modes of Atlantic SST departures. Contoured is the local percent variance explained by the respective modes with the sign of the spatial eigenvector. Arrows indicate the vector correlations of the surface wind anomalies with the temporal expansion coefficients for the respective modes; they are signed to indicate the associations with ocean warmings south (Figure 3a) and north (Figure 3b) of the ITCZ. The inset west of South America sets the scale for the vector field.

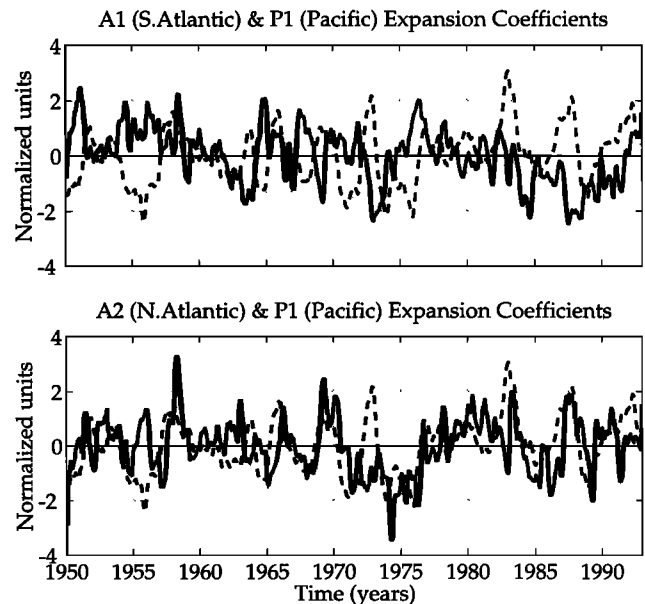


Figure 4. Normalized temporal expansion coefficients for the first two (A_1 , A_2) Atlantic EOF modes (solid curves) shown in relation to the first Pacific EOF mode (P_1 , dashed curve), computed from departures of SST (1950-1992).

cause the local variance explained within the A_1 and A_2 regions is so high, other techniques such as point correlation maps and crosscorrelation of simple area indices give equivalent results: indices of SSTA over these two sectors are poorly correlated and independent of the timescales of seasons to several years (i.e., interannual) that dominate this data set (all seasons combined). As we will discuss in later sections, however, small amounts of the SSTA variance may be anticorrelated across the ITCZ when particular seasons or geographical subsets are considered.

3.4. Interocean Correlations of SSTA

Comparison of the Atlantic SSTA modes with the dominant P_1 mode in the Pacific shows a highly significant positive lagged correlation (+0.5) with the North Atlantic mode (A_2), with the Pacific warmings preceding those of the Atlantic by 4–5 months. The negative correlation of -0.3 for the South Atlantic mode (A_1) with P_1 at a lag of 4 months is only marginally significant at about the 95% level. Both associations are for Pacific warmings with Atlantic warmings; the Pacific ENSO variability explains 25% of the North Atlantic modal variance, but only 9% of the South Atlantic. We presume that the unexplained variabilities (75% and 81%, respectively) represent processes that are intrinsic to the tropical Atlantic and are not related to Pacific-Atlantic teleconnections.

To better see how the ENSO-related SSTA variability is distributed in the Atlantic, consider the correlation pattern for the gridded Atlantic SSTA with the P_1 index at a uniform lag of 4 months (Figure 5). Correlation magnitudes above 0.2 exceed the 95% significance level. The strongest feature is the similarity of this pattern to that of the North Atlantic modal distribution (A_2 ; Figure 3b). The correlation is highest (above 0.5) in the same latitude band, 15°–22°N, and lowest (zero or slightly negative) off the African coast between the equator and 25°S. The region of lowest correlations corresponds to the region for which the negative South Atlantic mode (A_1) is strongest. This is consistent with the results of Zebiak [1993], who found negligible correlation between the NINO3 SSTA index in the Pacific and its Atlantic counterpart, ATL3 (3°S–3°N; 0°–20°W). Note that the dominant sense of the correlation pattern is not that of a dipole (opposite signs) across the ITCZ, although there is a tendency for weak anticorrelation

off SW Africa, which can also be seen in the A_2 mode (Figure 3b). Most of the correlation field in the South Atlantic is of the same sign as the North Atlantic. The suggestion is that the externally imposed ENSO forcing resonates with a natural mode of variability similar to A_2 , stronger in the North Atlantic and lacking any marked meridional antisymmetry.

Some differences are also apparent between Figures 3b and 5. Most notably, the region of highest P_1 correlation is skewed westward (toward the Caribbean) with respect to the A_2 pattern, which extends closer to NW Africa. A small region of secondary correlation (> 0.4) is found in the vicinity of the mean ITCZ position and east of 40°W. A third correlation zone (> 0.3) is oriented zonally along the 15°–30°S band between South America and the Greenwich meridian. The overlap between these two secondary regions and the A_1 pattern (Figure 3a) accounts for the small but significant negative correlation between P_1 and the A_1 modal series, noted above.

3.5. Wind Response to the Pacific ENSO

The vector correlations of the COADS surface wind with the P_1 Pacific ENSO index are superimposed on the scalar SSTA correlations (contours) in Figure 5. This is for a 1-month lag of the Atlantic with respect to the Pacific, for which the correlations are most often maximum (zero-lag correlations are very similar). That means that the vector wind correlations shown correspond to one season prior to the SSTA correlations contoured (4-month lag with respect to P_1). As we will see later, this is appropriate in view of the manner in which the SSTA connection is forced in the North Atlantic. The vectors indicate the sense of the anomalous winds associated with mature warm phases of ENSO oscillations. Comparison of this distribution with the seasonal means (Figure 2) shows that the SE trades south of the ITCZ are reinforced and a strong southerly component exists across and perpendicular to the axis of NE trades in the region where SSTA correlations are highest. There is also a strong anomalous flow from SE to NW across the mean position of the ITCZ. Other features include a large strengthening of the normal easterly flow from the Caribbean across the Isthmus of Panama and into the eastern North Pacific and a strengthening of easterly winds in the western equatorial Atlantic.

4. Variability by Seasons

4.1. Atlantic-Only SSTA Structures

Figure 6 shows the seasonal variability in the structure of Atlantic SSTA by highlighting the grid boxes for which the local variance explained by the two modes exceeds about 55% (60% for A_1 and 50% for A_2 , chosen for clarity). The EOFs are computed separately for the 3-month seasons centered on February (JFM), May (AMJ), August (JAS), and November (OND), and the total explained variance for the southern (A_1) and northern (A_2) modes is inset on the corresponding panels of the figure. The A_1 mode is always the more dominant, explaining 30–40% of the total variability over the year. The A_2 mode shows more seasonal variation, explaining more variance in the first half of the year (25–28%) and less than 20% during the second half. The respective regions of dominance tend to shift north and south with the seasons in a manner similar to the climatology of the SST field and the ITCZ latitude (Figure 2). The A_1 mode is usually dominant from the Gulf of Guinea (in AMJ, JAS, and OND) southward through a region off the coast of Namibia (20°–30°S). This structure is typified by the all-seasons analysis of Figure 3a. In JFM the A_1 mode retreats southward, leaving only a small area in the Gulf of Guinea that participates strongly with this mode. The A_2 mode is usually dominant in the central and eastern North Atlantic, also in

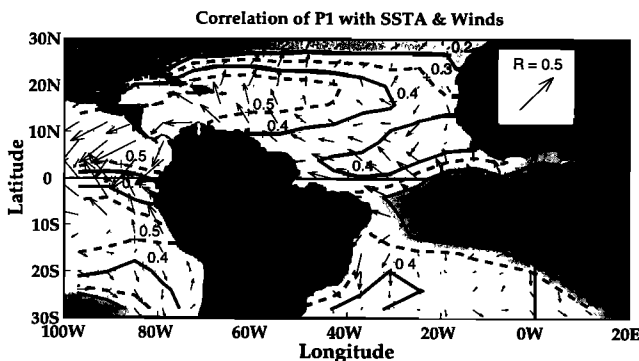


Figure 5. Vector correlation of COADS surface wind anomalies (arrows) and scalar correlation of SSTA (contours and shading) with the Pacific P_1 index. Correlations are for the full time series (all seasons) with SST lagging P_1 by 4 months and the wind lagging P_1 by 1 month. Lightest shading corresponds to the most positive correlations of SSTA, and darkest shading corresponds to the most negative correlations of SSTA. The inset over NW Africa sets the scale for the vector field.

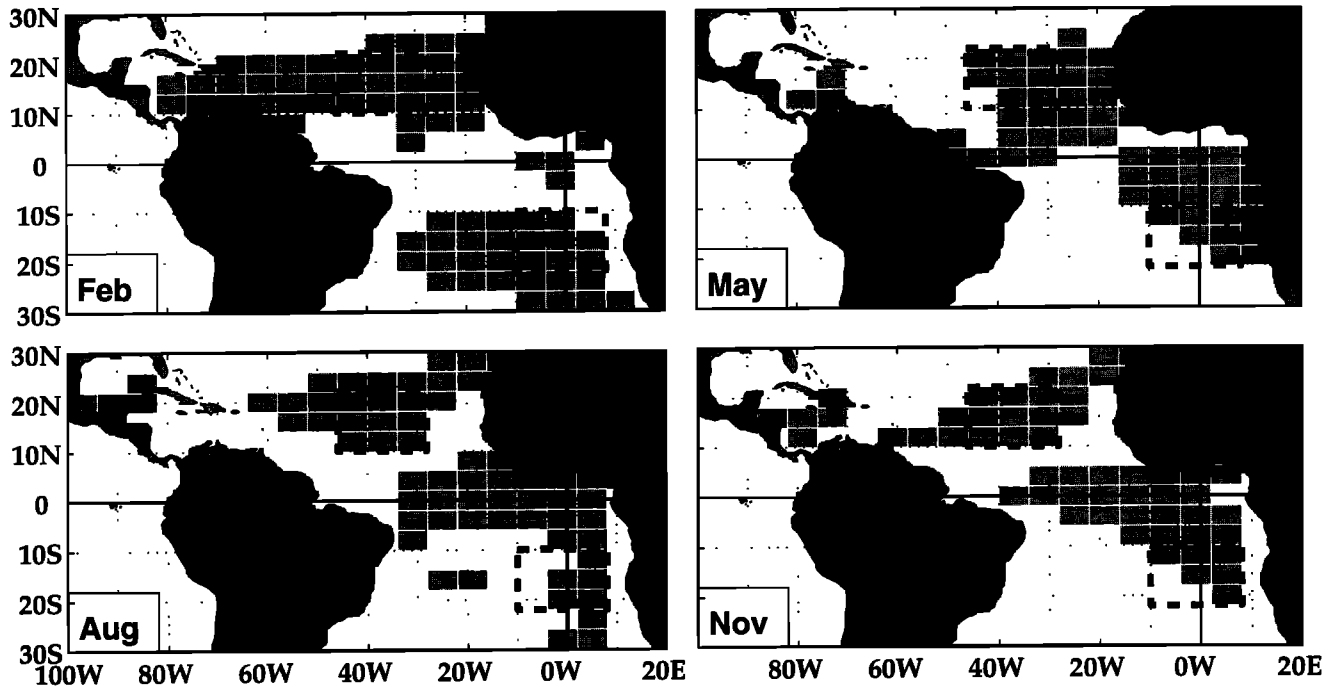


Figure 6. The 4×6 grid boxes where the A_1 and A_2 modes of seasonally calculated EOFs load highly are highlighted in gray. The A_1 region is highlighted where 60% or more of the local variance is explained and is always south of the seasonal mean position of the ITCZ, including the Gulf of Guinea and the equator; the A_2 region is shown for 50% or more of explained variance and is always north of the ITCZ. The total variance explained by the A_1 and A_2 modes is shown in the inset over NW Africa for each seasonal decomposition. The seasonal correlation of SSTA between area averages over the dashed boxes is inset over South America.

AMJ, JAS, and OND, but not in JFM when it extends all the way from NW Africa to Central America. However, in the case of A_2 it is the single JFM season that is best typified by the all-seasons structure (Figure 3b). This suggests that A_2 is more strongly influenced by one or two seasons, while A_1 varies less over the year.

Unlike other structural characteristics, the almost total lack of a dipole structure for all seasons combined (Figure 3) is changed marginally in the late boreal winter and early spring when there is a tendency for SSTA to be weakly anticorrelated across the ITCZ from the region where either EOF mode is dominant. This can be seen by calculating the correlation between two area averages of SSTA over the dashed boxes shown in Figure 6, chosen to maximize any anticorrelation present (correlations are shown numerically). The anticorrelation is of borderline (95%) significance in AMJ (-0.16), somewhat larger in JFM (-0.29), and nonexistent the rest of the year. The anticorrelation does not extend much beyond the small areas shown, and the correlation decreases as the size of the averaging boxes is increased.

4.2. Atlantic SSTA Versus Pacific ENSO (P_1)

The Atlantic SSTA correlations with P_1 (Atlantic lagging Pacific by 4 months) were also computed separately for the 12 calendar months of the year. The Pacific teleconnection pattern, for which Figure 5 is typical, has a very marked seasonality over the course of the year. It is most strongly developed in AMJ (Figure 7), transitional in JFM and JAS, and weak or absent in OND (not shown).

Over the calendar year the maximum positive and negative correlations remain in the range of 0.7 to 0.9 and -0.3 to

-0.6, respectively, not changing much from season to season (inset statistics in Figure 7). What better characterizes the seasonality in the teleconnection is the area over which the large positive correlations occur, north of the ITCZ, and the appearance of a small region of low (-0.25 to -0.35) but significant negative correlation near 5° - 10° S, 10° W in June, July and August. The latter feature is not spatially dissimilar from the weak anticorrelations noted in the SSTA structures (Figure 6) but occurs one-two seasons later. The wedge-shaped pattern extending westward from southwest Africa (defined by the dashed zero contour) continues through September and October, but the significant negative correlations are confined to a few hundred kilometers of the African coast, while the feature near 5° - 10° S, 10° W disappears. The negative correlations disappear entirely from the South Atlantic in November-December and begin to reemerge again in February. The weak anticorrelation near 5° - 10° S, 10° W during the boreal summer is the only manifestation of any tendency for the Pacific ENSO to induce a meridional dipole in the cross-equatorial SSTA structure of the Atlantic.

Also found in the South Atlantic, throughout the year, is a band of significant positive correlations of intermediate magnitude (0.35 to 0.55) extending eastward from Brazil, south of about 15° - 20° S. Thus the influence of the Pacific ENSO variability is pervasive in this region, without much seasonal dependence, but not as strong as its North Atlantic counterpart. As stated previously in relation to Figure 5, this positively correlated region is mainly responsible for the weak but significant correlation of the A_1 mode with the Pacific P_1 index.

Another area of significant negative correlation is seen in the northern Gulf of Mexico during February through May. This feature is absent during the rest of the year, but throughout

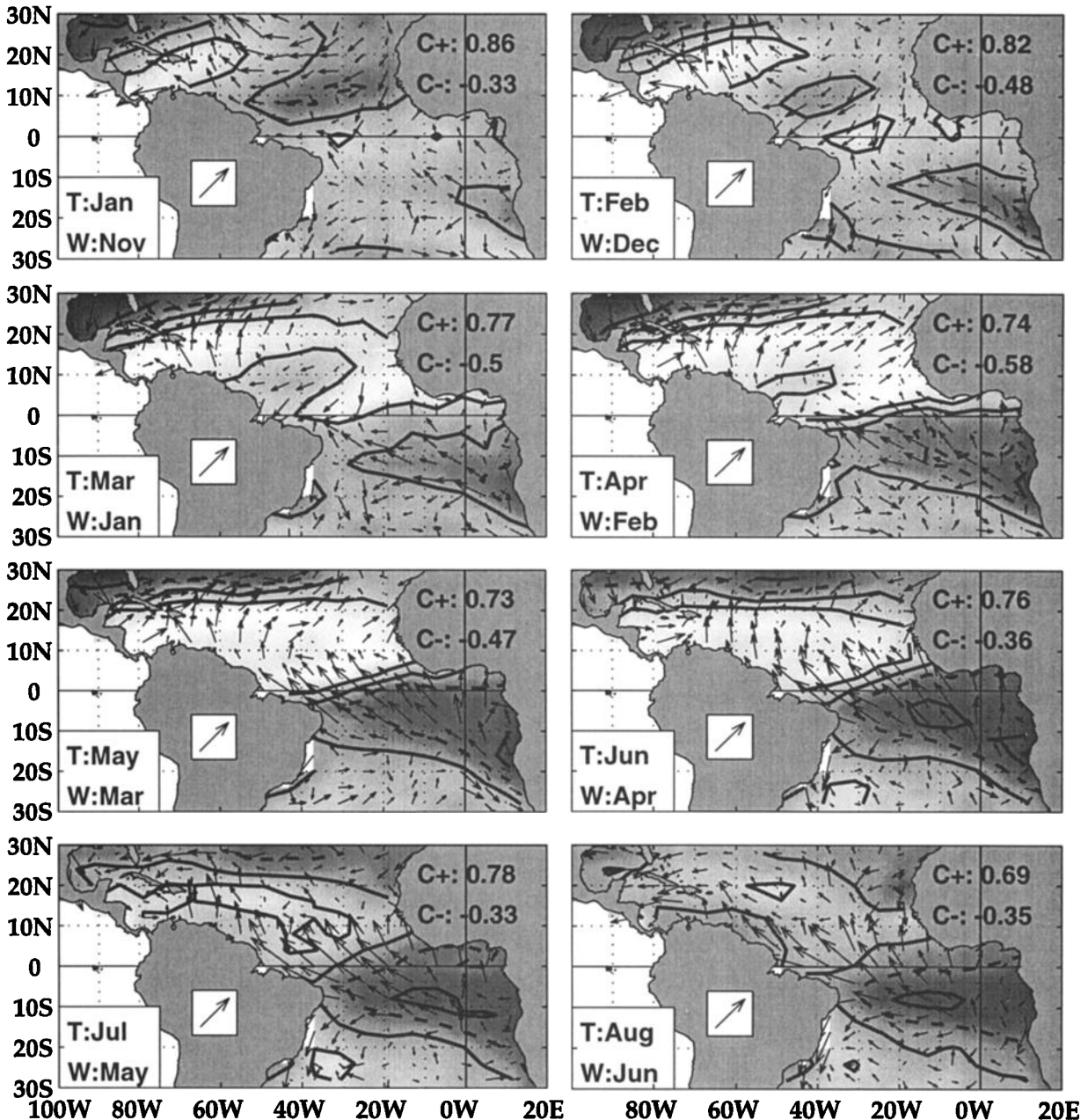


Figure 7. Distributions of the correlation of SSTA with the Pacific P_1 index (Atlantic lags by 4 months) are shown by contours and shading for 3-month running mean averages centered on the months of January through August. The lightest shading corresponds to the most positive correlations of SSTA, and the darkest shading corresponds to the most negative correlations of SSTA. Contours for SSTA are dashed for zero and solid at values of -0.25, 0.25, and 0.50 (95% significance = 0.25). The contemporaneous vector correlations of COADS surface wind anomalies with P_1 are shown by arrows for the months of November through June, i.e., 2 months prior to the corresponding SSTA distributions. The months for each panel are shown by the inset (lower left), with SSTA or winds denoted by a prefix of T or W, respectively. The inset over South America shows the magnitude for a vector wind correlation of 0.5.

most of the year, there is a characteristic northward gradient of correlation decreasing toward 30°N, with contours that typically extend eastward from the Gulf of Mexico to at least half the breadth of the Atlantic Basin.

The dominant and most interesting feature of Figure 7 is the large area of highly significant and numerically large positive correlations (above 0.6) during AMJ that extend from Africa to Central America and from the ITCZ to 20°–25°N. This pattern

weakens in July and is much weaker in the following 4 months, though still significant over a fairly large portion of the A_2 region. During most of JAS and OND the areally extensive correlations are somewhat less (0.4 to 0.6) and are restricted to a smaller region west of 30°W and north of 10°N. In December, January, and February the large positive correlations are confined mainly to the Caribbean region, and in March they expand again in a transitional configuration similar to July.

Another way to view the seasonality of the Pacific-Atlantic connections and also understand the timescales and lags involved is to examine the temporal distribution of lagged correlation between P_1 and seasonal subsets of Atlantic SSTA. In Figure 8, Atlantic SSTA in each of four seasons (represented by seasonal subsets of the A_1 and A_2 expansion coefficients in Figure 4) is correlated with P_1 for lags that vary monthly over a 2-year interval bracketing each of the seasons (dashed vertical lines). Correlations above 95% significance are found for the North Atlantic (A_2) lagging the Pacific (P_1) by 1-5 months. Consistent with the discussion of Figure 7, the largest correlation for A_2 (0.69) occurs in the boreal spring (AMJ) and the lowest (barely significant) occurs in late autumn (OND). The first half of the calendar year clearly contributes to most of the correlation pattern in Figure 5 (all months) and is best exem-

plified by January P_1 versus May A_2 . However, the JFM and AMJ seasons in the North Atlantic are significantly influenced by events in the equatorial Pacific during the entire preceding year.

Because the A_1 mode is negative, the negative lagged correlations of A_1 with P_1 indicate an overall positive correlation of South Atlantic SSTA with the Pacific ENSO, also consistent with the pattern for all months (Figure 5). As before, the negative correlations in Figure 8 appear to be mainly related to the geographical overlap between the southern portion of the A_1 pattern (Figure 3a) and the seasonally persistent band of positive correlations off southern Brazil (Figure 7). The strength of the lagged correlations of A_1 versus P_1 only exceeds the 95% significance level in late winter, with a 6-month lag at maximum (JFM); it is marginally significant in the seasons immediately preceding and following JFM and insignificant in the boreal summer (JAS). The latter season is when the area of insignificant and negative correlations off SW Africa (Figure 7) expands to occupy much of the A_1 region. It is this feature that mostly accounts for the seasonality in the A_1/P_1 correlations seen here, rather than seasonal variability in the band of positive correlations extending eastward from southern Brazil.

4.3. Wind vs. Pacific ENSO (P_1)

In section 5 we consider how the Atlantic SSTA is connected to the Pacific through thermal forcing by the surface winds. The wind-dependent thermal fluxes are contemporaneous with the SST tendency, such that they precede the maximum SST response by several months, thus accounting for the 4- to 5-month lags observed in the SST teleconnections. To understand the development of wind anomalies in relation to the SSTA evolution of Figure 7, we plot the contemporaneous vector correlation of the Atlantic surface winds with P_1 , 2 months prior to the corresponding SSTA season for each panel. Thus the panel for April SSTA shows the zero-lag wind correlation vectors with P_1 for the month of February, the May panel shows the correlation vectors for March winds, and so forth. This lagged juxtaposition of wind and SST correlations is done in recognition that the winds affect the SSTA tendency, which is presumably forced over the 4- to 5-month lag seen in the average P_1 -SSTA relationships (Figure 5). It is a somewhat arbitrary choice of lag and does not connote any special significance. In fact, we expect that the quickness of the SST response to imposed wind forcing will, in general, depend on the region and the processes involved. The following discussion refers to the effects of an ENSO warm phase, the sense of which is to produce SSTA anomalies of the sign shown and wind anomalies in the direction of the vector correlations. The implied sense of cold-phase effects is opposite.

During November through January the Pacific ENSO (as represented by P_1) is associated with southeasterly wind anomalies over the eastern Caribbean, veering to southerly in the region east of Cuba and Florida, while the anomalous wind distribution is anticyclonic over much of the tropical North Atlantic and similarly, but less well-defined, in the South Atlantic. The developing pattern of SSTA response begins in February with positive correlations over the Caribbean. In January, the SE trades begin to strengthen and there is anomalous convergence on the ITCZ from both sides, especially in the western equatorial Atlantic. By February and extending into March, the wind correlation pattern north of 10°N has extended across the entire breadth of the North Atlantic. Comparing the February vectors to Figure 2a, we see that wind speeds are decreased over most of the 10°-20°N band and increased to the north of 25°N. Consistent with the eastward expansion of the wind anomalies, the subsequent March and April SSTA patterns also extend to NW Africa along 10°-20°N. The February, March, and April wind patterns show further strengthening in the SE trades and a

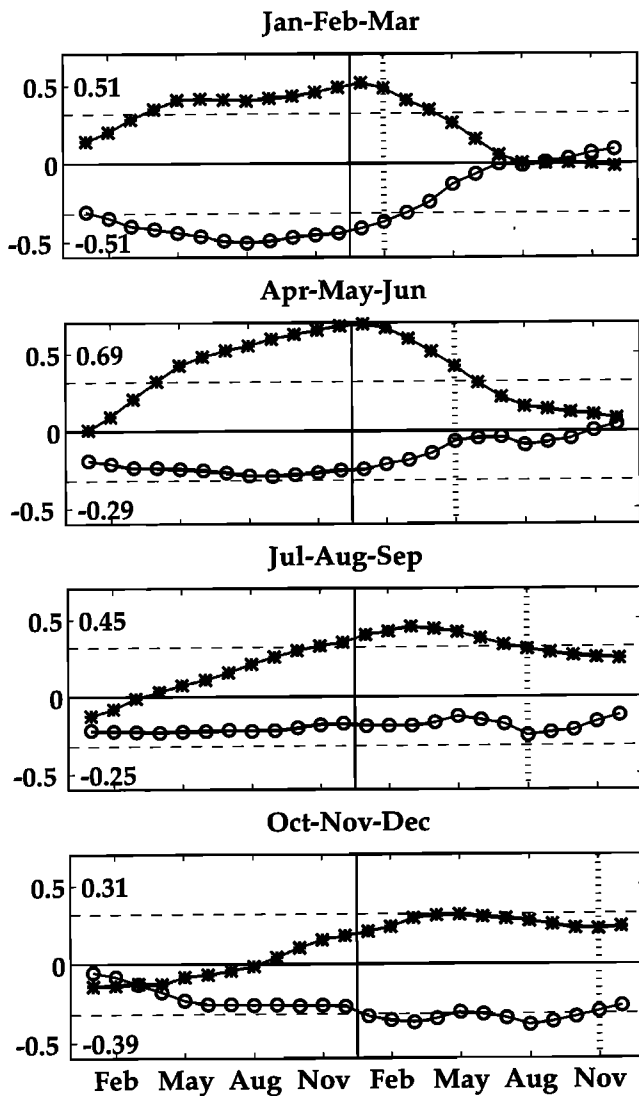


Figure 8. Seasonal values of the Atlantic modes (A_1 , circles; A_2 , asterisks) lag correlated with the P_1 mode during the same year (right half) and the prior year (left half). Positive correlations for A_1 imply that Atlantic cooling is associated with Pacific warming, and positive correlations for A_2 imply that Atlantic warming is associated with Pacific warming. Horizontal dashed lines are the 95% significance levels, and the numbers to the left are the most extreme correlations for A_2 (top number) and A_1 (bottom number). The seasons used are indicated by the vertical dashed lines and are labeled on the abscissa.

growing extension of SE wind anomalies across and perpendicular to the ITCZ and toward the North Atlantic region of anomalous increase in SSTA. The cross-ITCZ flow is consistent with an anomalous northward displacement of the ITCZ and is accompanied by a contemporaneous secondary zone of positive SSTA correlations along the northern flank of the mean ITCZ position in March and April. In April the North Atlantic SSTA pattern is well-developed, as is the anomalous flow across the ITCZ. By May the two bands of positive SSTA correlation have merged into a single large region between the ITCZ and 20°N. Finally, the SE trade anomalies become strongest in March through May and are followed one season later (JJA) by the appearance of negative SSTA correlations in the South Atlantic off Angola. Contemporaneously with these events the NE trade wind anomalies relax toward their normal configuration and the SSTA correlations in the North Atlantic weaken.

The qualitative impression we get from this sequence of events is as follows. As the warm phase of the Pacific ENSO cycle matures with maximum warming at the end of the calendar year, the NE surface trades weaken over the eastern Caribbean, quickly extending eastward to Africa and resulting in a warming over the 10°-20°N zonal band due to reduced cooling rates and lagged by one-two seasons with respect to the Pacific. As the North Atlantic warming intensifies, an anomalous flow from the South Atlantic across the ITCZ toward the area of warming quickly develops (winds lagging SSTA by 0-1 months). The associated northward displacement of the ITCZ is accompanied by a secondary warming parallel to and just north of the normal ITCZ position. The associated acceleration of the SE trades is followed several months later by a weak cooling pattern off Angola. The distributions of South Atlantic wind correlations also appear consistent with the development of anomalous anticyclonic wind stress curl over much of the subtropical gyre. The strongest component of the whole sequence and the one that leads all others is the broad SSTA correlation pattern between the Caribbean and Africa during April, May, and June. Understanding how that pattern is forced is the primary task of the next section.

Correlations may, in some situations, be misleading. If, for example, the effects of ENSO cold phases do not mirror (in an opposite sense) those of warm phases, correlations may not reflect either situation accurately. To check on this, we identified sets of years with positive (10 events) and negative (eight events) extremes in the P_1 series (Figure 4) that reach 1 standard deviation or more, and constructed composite averages of wind and SST anomalies for each set, mapped over the months corresponding to those shown in Figure 7. Both the warm-phase set and the cold-phase set reproduce the principal relationships shown in Figure 7 but reversed in sign with respect to each other. We conclude therefore that the correlation format chosen in Figure 7 represents both phases well. The composite analyses additionally show that the average SSTA response for either ENSO phase exceeds 0.3°C over areas where the SSTA correlations (Figure 7) are significant. They exceed 0.5°C in more limited regions surrounding the coastal upwelling systems of NW and SW Africa where SSTs are coldest in the mean and their variance the greatest.

5. Forcing Mechanisms

5.1. NE Trades (A_2) Region

We can plausibly hypothesize that the ENSO signal from the Pacific initially influences the Atlantic SSTA variability through a tropospheric connection along 10°-20°N. Interest in the ENSO effects on hurricane frequency has already led to the discovery that tropospheric vertical wind shear in the tropical North Atlantic increases in conjunction with ENSO warm

phases [e.g., Gray, 1994]. That relationship, however, mainly involves a strengthening of the westerly wind flow in the upper troposphere during the boreal summer, while the easterly low-level flow at a height of 2 km remains normal. In the case of the strongest SSTA correlations under the NE trades, the most likely connection is through some aspect of the surface wind field during the boreal winter, as suggested by Figure 7. Radiational heat flux terms seem less likely because most of this region involves neither low-level stratus decks nor convective convergence bands where cloudiness changes could be a major factor in the surface heat balance. This would not be true, however, of the ITCZ region farther south where convective activity is ubiquitous.

Most of the heat flux divergence terms that can increase the mixed layer heat content in response to surface winds can be wholly or partially estimated from the COADS data base. One that cannot, for example, is the large-scale SST advection by geostrophic flows that are altered on the basin scale. This would require data capable of estimating large-scale subsurface pressure gradients, such as expendable bathythermograph (XBT) profiles. Unfortunately, the available XBT data are insufficient for resolving the nonseasonal variability over our period of analysis. However, most studies tend to confirm the Bjerknes [1964] hypothesis that such a mechanism operates preferentially at longer timescales and that variability on the interannual timescales seen here is forced mainly by local surface fluxes [e.g., Halliwell and Mayer, 1996]. We therefore use the COADS data to estimate the following heat flux divergence terms (right side) that locally affect the mixed layer temperature tendency (left side) and can be wholly or partially estimated from surface observations:

Latent heat transfer

$$\frac{\delta T'}{\delta t} \propto -W' \langle \Delta q \rangle - \langle W \rangle \Delta q' \quad (1)$$

Sensible heat transfer

$$\frac{\delta T'}{\delta t} \propto -W' \langle \Delta T_a \rangle - \langle W \rangle \Delta T_a' \quad (2)$$

SST advection by Ekman flows

$$\frac{\delta T'}{\delta t} \propto \frac{\overline{V'_E} \cdot \nabla T'}{E} \quad (3)$$

Ekman pumping (vertical advection)

$$\frac{\delta T'}{\delta t} \propto \nabla \times \frac{\overline{\tau'}}{f} \quad (4)$$

Entrainment (wind power)

$$\frac{\delta T'}{\delta t} \propto W'^3 \quad (5)$$

where T , ΔT_a , Δq , W , V_E , and τ refer to the ocean mixed layer temperature (represented by COADS SST), surface air temperature difference (surface minus 10 m), specific humidity difference (surface minus 10 m), wind speed, Ekman velocity (averaged over the mixed layer), and surface wind stress, respectively. Angle brackets denote time averages (climatological annual cycles unless otherwise noted) and primed quantities are the departures from those averages. It is assumed that V_E can be represented by the Ekman transport (τ/f); this is only an assumption of proportionality for the correlation analyses done in this paper. Note that the evaporative and sensible heat flux terms are decomposed into the contributions from anomalous wind speed (W') and anomalous lapse

rate ($\Delta T_a'$ or $\Delta q'$), respectively. It has been shown by Frankignoul [1985] that SST is forced at short timescales by the former while the latter acts on long timescales as a feedback or restoring mechanism. Because we are specifically interested in the ocean-forcing aspects of the fluxes, the estimates of latent and sensible heat transfer ((1) and (2)) are done without the feedback term.

Except for known or estimated bulk aerodynamic coefficients, the first three relationships summarize the COADS derivable information that completely specifies the effect of the appropriate term on the tendency of mixed layer temperature anomaly. The fourth relationship is essentially the near-surface vertical velocity in the vertical advection term and does not account for changes due to variability in the depth or intensity of the thermocline. The fifth relationship characterizes the cooling due to entrainment across the mixed layer base, which is greatly (but not completely) influenced by the rate of dissipation of mechanical energy from the wind (wind power $\propto W^3$). There too, the effects of changes in stratification on entrainment cooling cannot be accounted for using the COADS data.

The search for ENSO forcing terms relies on two types of analysis. First, the right-side forcing terms are computed from the COADS summaries (most terms) and the raw COADS data (W^3 term) in 2° bins over the Atlantic. Their correlations with the tendency of the North Atlantic SSTA mode ($\delta A_2/\delta t$) during the ensuing month (forward time difference) are mapped. If a term is normally important in forcing the North Atlantic, we expect to see a spatially coherent pattern of significant correlation of the appropriate sign over the region where the A_2 pattern is strong (Figure 3b), indicating that the flux divergence term contributes significantly to the colocated anomalous

temperature tendency. Second, we correlate the same right-side term with the P_1 (equivalent to NINO3) index and check for spatially coherent correlations in the North Atlantic region where SSTA is strongly correlated with P_1 (Figure 5). The presence of *both* patterns is taken to mean that the flux divergence term in question probably contributes significantly to the tropospheric forcing of the ENSO-related SSTA variability. The final element of plausibility for a particular forcing term is to find a seasonal march and a lag with respect to SSTA and vector wind correlations (Figure 7) that are also consistent with the candidate forcing mechanism.

The results discussed below are for seasonal (3-month) averages centered on each of the 12 calendar months. Having checked their representativeness, we display the results for simple wind speed anomalies (versus A_2 and P_1) as a proxy for the heat flux terms involving that variable, namely the latent and sensible heat terms ((1) and (2)) (for which the patterns are virtually identical) and the wind power (so similar that the conclusions are unaffected). Comparisons with the wind anomalies show that the changes in these surface flux terms are entirely due to the anomalous variability of the surface winds and not to the climatological lapse rates of moisture or air temperature.

The effects of wind speed-related heat losses on the A_2 tendency are shown in Figure 9 by the correlation fields for W' with A_2 , for the 4 months from December through March. These are months for which the significant A_2 forcing pattern appears to be much stronger than during the rest of the year. The pattern is clearly dominated by the extensive region of large negative correlations (darkest shading, -0.2 to -0.7) between Africa and the Caribbean. The geographical correspondence of this region to the region of A_2 dominance (Figure 3b), plus its persistence over these 4 months, is con-

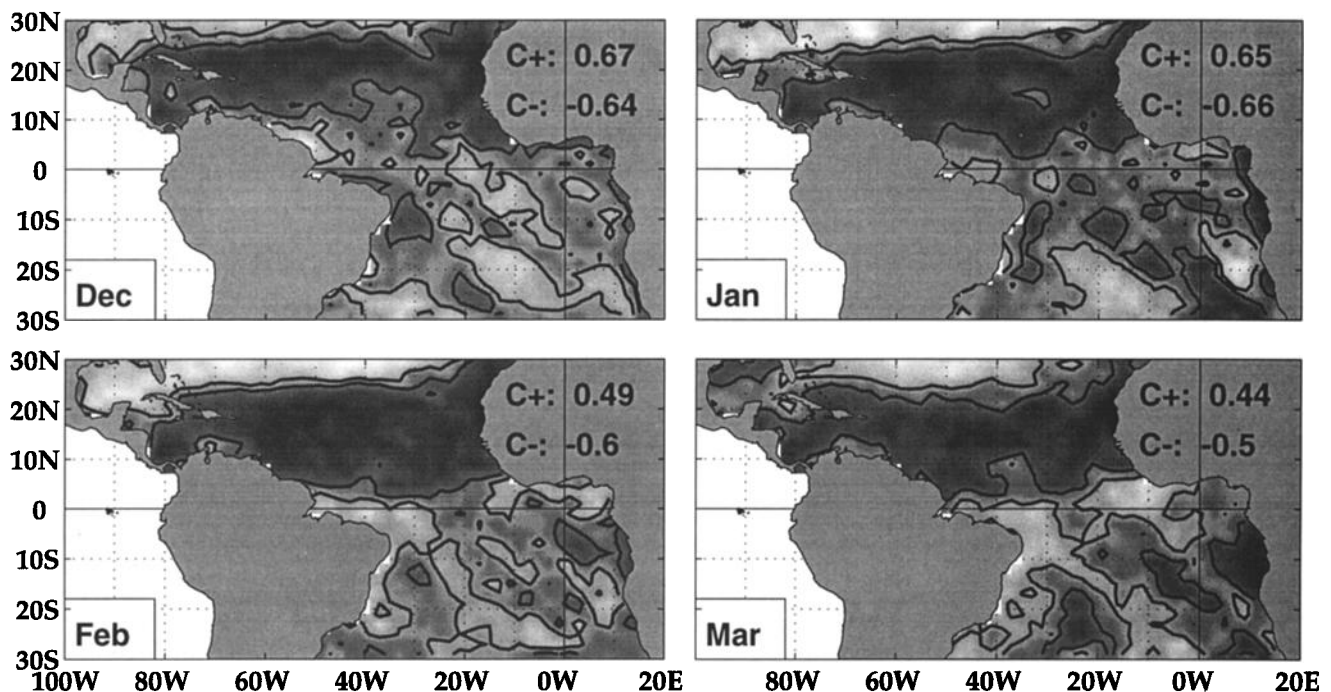


Figure 9. Zero-lag scalar correlations of the wind speed anomaly with the tendency of the temporal expansion coefficients for the North Atlantic mode ($\delta A_2/\delta t$), for 3-month averaged fields centered on December through February. Lightest shading corresponds to the most positive correlations, and darkest shading corresponds to the most negative correlations. The 95% significance level is 0.12. Solid contours separate correlations at or above that level (dark and light shading) from insignificant values (medium shading). The extreme positive and negative correlations in each field are inset over NW Africa.

sistent with a positive tendency in A_2 , being related to reduced cooling from the fluxes affected by wind speed: evaporation, sensible heat, and entrainment. Furthermore, the large region of negative correlation between NW Africa and the Caribbean is consistent with a strong A_2 pattern that is zonally extensive during the late boreal winter (Figure 6).

A secondary region of significant positive correlations, strongest in January and February (+0.2 to +0.7), extends along the northern boundary of the data domain (25°–30°N) and into the Gulf of Mexico (Figure 9). Another pattern of positive correlations appears off NE Brazil in February, extends farther eastward into the western Gulf of Guinea in March, and covers that entire region in May, June, and July (not shown). However, both of these regions of positive correlation are located on the fringes of the A_2 pattern where the local variance explained by that mode is quite low (Figure 3b). This, plus the fact that the sign of the correlation is not consistent with local forcing, indicates that these are regions where the wind speed anomalies are anticorrelated to those over the central North Atlantic but where the A_2 mode is not being locally forced.

The January through April correlations of W' with P_1 (Figure 10) show a positive-negative-positive pattern between the western equatorial Atlantic and the western Atlantic north of 25°N, extending into the Gulf of Mexico. The pattern is persistent and very similar to the pattern that associates W' with A_2 tendency (Figure 9). The large region of significant negative correlations (-0.2 to -0.7) between 20°W and the Caribbean indicates that evaporative heat loss is diminished there in association with warm phases of the Pacific ENSO variability. This is consistent with the collocated positive correlation between P_1 and lagged SSTA (Figures 5 and 7). The significant positive W' correlations north of there are similarly consistent with the collocated ENSO-related cooling that spans the Gulf of Mexico and the region just east of Florida.

The patterns shown are also similar to, but more intense than, the patterns for all months combined (not shown). Hence the relationships that lead to the P_1 correlation pattern of Figure 5 (all months) are strongly seasonal and mainly op-

erative between December and April. This seasonality is consistent with the seasonal development of wind and SST anomalies discussed in reference to Figure 7. Other than the features already noted in Figures 9 and 10, the patterns during the rest of the year show no relationships that persist over any extensive region and are also present in both plots.

As with the evaporative and sensible heat loss, the associations with wind power (not shown) are very similar to those of wind speed (Figures 9 and 10), a fact attributable to the relative steadiness of the NE trades, such that $\langle W'^3 \rangle \approx \langle W' \rangle^3$. However, because the wind speed is a complete proxy for the latent and sensible heat terms in the A_2 region, while the entrainment term is incompletely specified, a comparison of their respective correlation structures cannot account for the importance of the latter process relative to the former. All three terms are of the same sign and probably contribute to the ENSO-related thermal changes in the mixed layer. Over the tropical North Atlantic the ratio of sensible heat transfer relative to evaporation is normally less than 1/20 [Esbensen and Kushnir, 1981]; hence the contribution of the sensible heat flux is probably no greater than the uncertainties in the data. However, the relative contributions of wind-related evaporation and turbulent entrainment are less clear. Recent model simulations indicate that both terms contribute significantly to the normal mixed layer heat balance but that the contribution from the evaporation term is greater (G.R. Halliwell, Jr., Simulation of North Atlantic decadal/multi-decadal winter SST anomalies driven by basin-scale atmospheric circulation anomalies, submitted to *Journal of Physical Oceanography*, 1996). Hence it is reasonable to suggest that both evaporation and entrainment are important and that evaporation is probably the more vigorous mechanism.

What appears to best characterize the signal input from the Pacific, through the wind field, is the persistence of significant correlations over a fairly large area and for an extended period of several months or more. To show this, Figure 11 maps the prevalence of correlations (P_1 versus W') larger than the 95% significance level, where prevalence is defined to be the num-

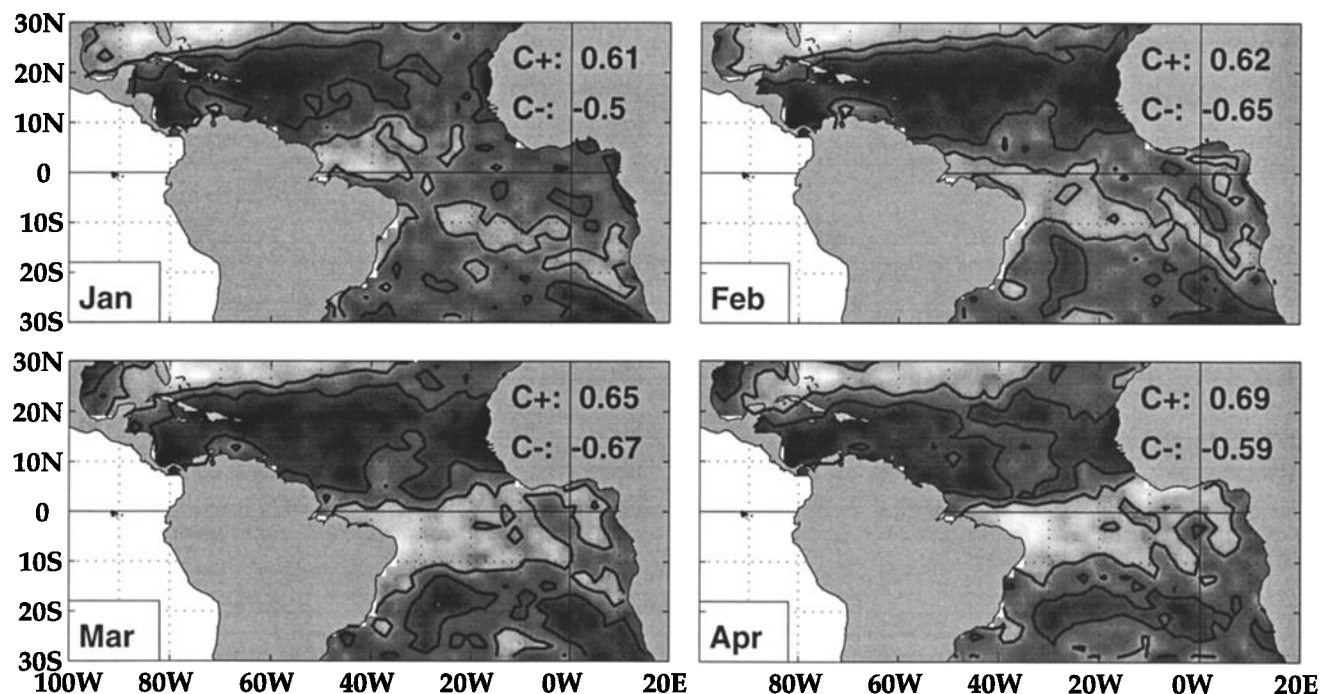


Figure 10. As in Figure 9, but for wind speed anomaly versus P_1 , and for the seasons centered on January through April. The 95% significance level is 0.16.

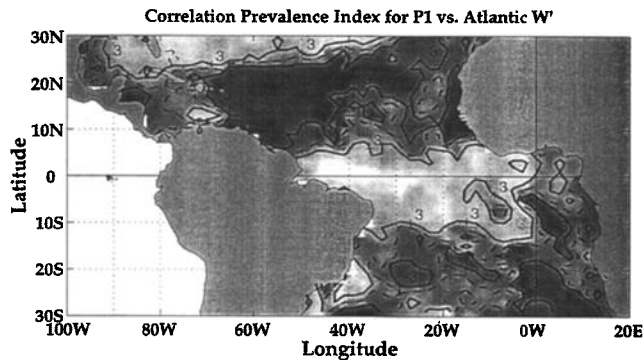


Figure 11. Distribution of the correlation prevalence index, defined as the number of calendar months for which the P_1 /wind speed correlation exceeds the 95% significance level. The dashed contours are for zero, and the contours of ± 3 months surround regions of high prevalence for positive (light shading) and negative (dark shading) correlations.

ber of calendar months for which the condition is satisfied. The three areas that stand out are the ones already discussed in relation to Figure 10, with a prevalence of 3 months or more: the large zonal region of negative correlation centered near 20°N and the the regions of positive correlation immediately to the north (25°–30°N) and south (10°S to 5°N). These regions are also persistent; that is, the months of prevalence are also consecutive months in the late winter and early spring (two northern zones) or spring and early summer (equatorial zone). There is a smaller region of contiguous negative prevalence in the South Atlantic, but values in excess of three occur only over several small patches of ocean.

The forcing terms due to Ekman pumping and ageostrophic (Ekman) advection ((3) and (4)) show no compelling patterns for any of the seasons, and we conclude that they are of no importance to A_2 . Finally, the same analyses, applied to the A_1 tendency, yield no significant and mutually consistent correlations for the forcing terms over all months. Hence we cannot conclude that the A_1 pattern responds to local surface fluxes in the way that A_2 does.

5.2. Convergence Region

There may be a basis for discriminating between the processes (discussed above) that affect the broad east-west region north of 10°N and the region of secondary SSTA correlation with P_1 (Figure 5) that extends in a WSW-ENE direction between 40°W and the African coast and lies closer to the northern limit of seasonal ITCZ activity than to the southern limit (Figure 2). Unlike the core region of the trades in either hemisphere, the ocean-atmosphere interactions in convergence zones characteristically involve a convective-radiative equilibrium in the planetary boundary layer that is associated with warmer water under the surface wind convergence. This can be clearly seen in Figure 2 where the confluence in the meridional component of the wind is collocated with the axis of warmest water and with the maximum ITCZ convergence calculated from the COADS wind data. The ENSO-related wind anomalies in this region (Figures 5 and 7) are directed toward the NW, are perpendicular to the ITCZ, and are consistent with an anomalous northward shift in the position of both the convergence and the warmer water.

The likelihood that this is occurring can also be seen in the seasonal evolution of the SSTA and wind speed relationships (Figures 7, 9, and 10). Sharp boundaries between regions of negative (north) and positive (south) wind speed correlation

characteristically occur near the ITCZ axis in February–March (Figure 9) and March–April (Figure 10), consistent with weakened winds just north of the ITCZ confluence and strengthened winds just south of the ITCZ confluence. In March and April (Figure 7), the SSTA shows a separated correlation pattern in the secondary region of Figure 5 that merges with the broad A_2 pattern near the NW Africa coast. Later in the boreal spring the two regions merge completely.

To independently test for this relationship, the latitude of maximum convergence (negative divergence) was calculated from the COADS wind data along the 29°W meridian. There is a 90% significant positive correlation (+0.15) between the ITCZ latitude anomaly at 29°W and the P_1 variability. The correlation is quite low, explaining very little of the ITCZ variance. This is not particularly surprising in view of the generally noisy character of the COADS winds (compared with the reconstructed SST) and the fact that they are differentiated in order to produce the divergence field. Even so, the weakness of the correlation suggests that the Pacific teleconnection does not explain much of the total nonseasonal ITCZ variability. The relationship appears significant, however, such that together with other indications it is consistent with a northward bias in the convergence location and supports an ITCZ mechanism for explaining the collocated SSTA correlations with P_1 . The northward shift is in turn probably induced by the primary ENSO-related warmings in the A_2 region farther north.

We have been unable to explore comparable relationships in the SACZ region off southern Brazil because the latter region is one of relatively poor COADS coverage and the wind divergence there is too diffuse and noisy for making reliable estimates.

5.3. Western Equatorial Atlantic

One notable feature of Figure 5 is that the positive SSTA correlation in the western equatorial Atlantic is weakest between the equator and 10°S off NE Brazil. The easterly component of the overlying wind field there is enhanced in association with Pacific ENSO warm phases (correlation with the NINO3 index is -0.24, significant at the 99% level), and the wind speed anomalies are positively correlated there from February through June (March–April in Figure 10 are typical). Therefore the positive correlations of P_1 with SSTA off Brazil are generally inconsistent with forcing by heat fluxes related to wind speed, although whatever produces the warmings there appears to be partially offset by those fluxes in the region of minimum correlation. It seems likely that the positive SSTA correlations north of the equator (off Brazil) are also associated with the ITCZ process mentioned above. South of there, however, we can only speculate that the positive correlations are due to an advection process. For example, as in the western Pacific, enhanced easterly winds near the equator may be associated with the accumulation of upper layer water in the west, an increase in thermocline depth, and a slight warming. Such a process would also argue for an analogous cooling in the Gulf of Guinea due to a shoaling of the thermocline in the east, accompanied by increased cooling due to entrainment. The only time of year when negative SSTA correlations (with P_1) extend over that region is in June and July (Figure 7). While that is qualitatively consistent, both in terms of sign and the time of year, the correlations are weak and not significant.

5.4. South Atlantic

The situation at the higher latitudes of the South Atlantic is far less clear than in the North Atlantic. On the one hand, there is a tendency for SSTA in the region west of Angola to be minimally correlated with P_1 in April–May and negatively correlated during June through August (Figure 7), and for the SE

trades over the same region to be strengthened in connection with ENSO warm phases (Figure 5, all months). Although this would seem to be consistent with an increased heat loss due to evaporation, the wind speed correlations for specific months (Figure 10) do not bear this out. On the other hand, there is a clear tendency for warmer SSTs to be associated with ENSO warm phases in the 20°-30°S band extending eastward from southern Brazil (Figures 5 and 7). While wind speeds tend to be negatively correlated with P_1 along 15°-25°S, the geographical fit with the SSTA pattern is not very good (Figure 10) and the prevalence of negative correlations is considerably less than we see in the A_2 region (Figure 11). We note, however, that the COADS data are less dense in the South Atlantic and preferentially distributed along or near ship routes which can lead to choppy correlation patterns. Thus wind-related heat flux forcing such as we see in the North Atlantic does not offer a satisfactory explanation for the South Atlantic SSTA structures.

There may exist alternative explanations for the positive SSTA correlations in the South Atlantic. Although to test the influence of advective heat transports is beyond the scope of our study, the observed vector correlations of the SE trades with P_1 (Figure 5) are consistent with a large-scale anticyclonic wind stress curl anomaly over much of the subtropical gyre. Transport changes in the gyre components (Brazil Current, Benguela Current, and South Equatorial Current) would not have to be large to produce SST changes of up to a degree (only a few centimeters per second of velocity change are needed). The sense of the observed SSTA correlation pattern is qualitatively consistent with such a mechanism, with cooling over the northeast limb of the gyre and warming over the southwest limb of the gyre being associated with an accelerated circulation.

6. Summary and Discussion

The results of this study can be summarized as follows. Taken without regard to the Pacific ENSO or to season, interannual SST variability in the tropical Atlantic is independent between the regions north and south of the ITCZ (no dipole). In the boreal spring, a small region west of Angola and northern Namibia exhibits a tendency toward anticorrelation with the tropical North Atlantic, but only a small fraction of the SSTA variance is involved.

As ENSO warm phases culminate around December-January in the equatorial Pacific, persistent and spatially coherent decreases in wind speed occur over an extensive region of the NE trades from NW Africa to the Caribbean, resulting in reduced heat loss in the surface mixed layer due to evaporation and entrainment. This induces a positive anomaly of SST tendency that persists for several months, culminating in tropical North Atlantic warming in the late spring and early summer, one-two seasons after maximum anomalies in the Pacific. These events also appear to be associated with a northward shift in the latitude of the ITCZ with consequent warming immediately north of the mean ITCZ position and weak cooling to the south. Consistent with the warming in the tropical North Atlantic and the ITCZ shift, anomalous winds are directed across the ITCZ from SE to NW, resulting in stronger SE trades at low latitudes in the South Atlantic. Then, in June and July, a weak tendency for cooling occurs in the region of SE trade anomalies west of Angola, and a strong tendency for warming occurs in a 20°-30°S band east of southern Brazil and spanning much of the South Atlantic. The South Atlantic SST anomalies are not strongly related to local surface heat fluxes as in the North Atlantic but appear to be qualitatively consistent with a strengthening of the South Atlantic subtropical gyre circulation. The latter is speculation, however; we cannot conclusively exclude

local forcing effects because of the comparatively poor COADS data coverage in the South Atlantic.

6.1. Regarding the Atlantic SST Dipole

There is confusion in the literature on the issue of meridional SSTA structures in the Atlantic. A number of studies have pointed to dipole (meridionally anticorrelated) behavior [e.g., Weare, 1977; Hastenrath, 1978; Moura and Shukla, 1981], while others do not [Houghton and Tourre, 1992]. Our results tend to support the findings of Houghton and Tourre [1992], who show that under a varimax rotation, the EOFs of tropical Atlantic SSTA (20°S to 30°N) separate into independent north and south modes and that nonseasonal SST does not behave as a meridional dipole. Their EOFs, prior to rotation, are not stably separated and showed a dipole pattern in the second EOF, similar to the results of Weare [1977]. Choices regarding the geographic and temporal domains and data normalization seem to account for the differences between our respective EOF structures (R. Houghton, personal communication, 1995). In the patterns for this study (Figure 3) and in the rotated patterns of Houghton and Tourre [1992], the two modes are stably separated, the dipole disappears, and the local explained variance increases in the A_1 and A_2 regions.

The local explained variance in the A_1 and A_2 regions is so large that the conclusions regarding modal independence extend also to simple large-area averages. Lagged cross correlations (all seasons) between large-area averages in the two regions are insignificant out to lags of 15 months, confirming that there is very little dipole effect in the SSTA at the interannual timescale that dominates the Smith *et al.* [1996] data set. We note, however, that this independence does not necessarily apply to interdecadal periodicities where the timescale matches that of large-scale coupled processes that are not yet understood. Recent work by Mehta and Delworth [1995] confirms the lack of dipole behavior at interannual periodicities but also indicates its existence at periods in excess of about 12 years. Similar results are seen in the modeling study by Huang *et al.* [1995].

Although our first-order results contrast with studies that show dipole behavior, the discrepancies can be explained. In the case of the SST analyses done previously [Weare, 1977; Hastenrath, 1978], the unrotated EOFs are sensitive to choices for the data domain and may decompose into poorly separated, unstable modes that do not explain local variability as strongly as do the rotated modes. In climate-oriented analyses [e.g., Moura and Shukla, 1981; Folland *et al.*, 1986], dipole behavior typically appears when the SSTA variability is correlated or composited with respect to response variables that are sensitive to north-south SST gradients and anomalous ITCZ movements, such as NE Brazil or NW Africa rainfall. Analyses of this type are done to gain insights into the terrestrial climate response; they cannot be compared to analyses of SST alone, and they cannot be used to infer that the internal ocean dynamics or even the ocean-atmosphere interactions are inherently dipolar in nature.

Although the dominant tropical SST variability is primarily nondipolar, the reader will recall that a weak tendency toward meridional antisymmetry is seen in the small loadings of opposite sign in the A_2 distribution south of the equator (Figure 3b). Only a small region along the coast of Angola (15°-20°S) has up to 20% of the explained local variance with the opposite sign. There is also a seasonal character to this tendency, whereby the SSTA in the region west of Angola tends to be weakly (but significantly) anticorrelated with the tropical North Atlantic in the boreal late winter and early spring (Figure 6), while the Pacific ENSO signal tends to induce a similar weak dipole structure in the summer months (June through August in Figure 7). This implies a tendency for

nearshore waters to cool in conjunction with increased southerly winds and coastal upwelling, when the A_2 region off NW Africa is warmer than normal. This is consistent with the vector wind correlations with A_2 (Figure 3b). The very weak negative loadings for A_2 over the larger SE trades region are consistent with an SST response to the larger scale southerly wind anomalies associated with A_2 , possibly through the mechanism proposed by *Philander and Pacanowski* [1981]. The associated anomalous wind stress curl over the South Atlantic may also cool or warm this region through advective changes in the subtropical gyre circulation.

The results are also largely consistent with the findings of *Huang et al.* [1995], who observe the behavior of an Atlantic general circulation model forced by observed winds for the period 1980-1988. This is a comparatively short period in which a strong interdecadal swing took place. Their leading mode of a singular value decomposition (SVD) analysis between SSTA and anomalous winds shows a mutual relationship between the two fields that is very similar to what we have described, with warmings in the A_2 region being associated with weakened NE trades and increased SE trade flow extending NW across the ITCZ, plus easterly anomalies in the western equatorial Atlantic. However, the SVD mode shows a much stronger anticorrelation in the South Atlantic SSTA than what we see with our much longer data set, which is dominated more by interannual variability. The *Huang et al.* [1995] modal time series show that most of the associated variability is due to the strong interdecadal shift. Hence the ocean-atmosphere relationships appear to be very similar between the two timescales, but the tendency toward dipole behavior in SSTA is much stronger at the longer timescales.

6.2. Response of SSTA to ENSO

As stated before, this study most strongly supports previous work, such as *Hastenrath et al.* [1987] and *Hameed et al.* [1993], in the tropical North Atlantic. We agree that the North Atlantic warms in response to the Pacific ENSO and that the effects in the North Atlantic are stronger. To this we add that the North Atlantic lags the Pacific by about one-two seasons and that the ENSO response in the Atlantic has a fairly marked seasonality, being strongest in the boreal spring and early summer and weakest in the fall and early winter. For the South Atlantic, the *Hastenrath et al.* [1987] results suggest that the principle impact on SSTA is opposite to that of the North Atlantic. Our results indicate that the strongest SSTA correlations in the South Atlantic are of the same sign as for the North Atlantic (Figures 5 and 7) and they are shifted toward the western side of the basin. However, eastward from South America the correlations weaken and eventually become weakly negative off Angola and Namibia, in a manner very similar to the A_2 pattern. To first order, then, the SSTA response to ENSO is not meridionally antisymmetric. However, the occurrence of cooling off Africa could certainly lead one to conclude that the ENSO response is weakly antisymmetric, depending on where area indices are computed.

The ENSO-related events in the Atlantic show a clear seasonal structure and a temporal progression from north to south. For reasons that are beyond the scope of this paper to address, the most extensive and spatially organized anomalies in the low-level Atlantic wind field occur first in the tropical North Atlantic during the late boreal winter and early spring, shortly after the maximum SST anomalies in the Pacific. The associated reductions in wind speed and upper ocean cooling result in maximum North Atlantic SSTA in the late spring, leading into the summer season of maximum absolute temperatures (Figure 7). The spring is also the season for which trade wind

dominance normally shifts from the North Atlantic to the South Atlantic and the ITCZ migrates northward (Figure 2). The effect of positive SST anomalies in the North Atlantic is to cause an early spring transition, and the effect of negative SST anomalies in the North Atlantic is to cause a late spring transition, with resulting changes in the strength of the SE trades in the early boreal summer. The distribution of the SE trade anomalies is consistent with changes in the large-scale pattern of wind stress curl over the South Atlantic. The sense of the wind stress curl anomaly is such as to produce an altered subtropical gyre circulation consistent with the observed South Atlantic correlations of SSTA with P_1 during the boreal summer (Figure 7). Because of the relatively short delay between the SE trade anomalies and the resulting SSTA pattern, the most likely mechanism is that of a mostly barotropic gyre response to an altered Sverdrup balance.

The scenario for changes in the South Atlantic is only a plausible speculation at this point. However, the features associated with ENSO warm phases (the warming off Brazil, the cooling off Africa, and the stronger SE trades) and the proposed mechanism linking them, are all consistent with the *Hameed et al.* [1993] conclusion that the North Atlantic warms in response to ENSO, while the subtropical high-pressure system and associated trade circulation are strengthened in the tropical South Atlantic.

The one-two season lag in the Atlantic SSTA response to ENSO can best be understood in terms of the greater thermal inertia of the ocean compared with that of the atmosphere and of the different ways in which the two media force each other. The tropospheric response to peak anomalies of SST in the Pacific is nearly contemporaneous. We consistently see correlations of Atlantic winds with P_1 that are maximum at lags of 0-1 months. However, the Atlantic SSTA response is time shifted because the wind forcing must be contemporaneous with the local SSTA tendency, which in turn is time integrated to culminate in maximum SSTA on a timescale consistent with the duration of maximum anomalies in the Pacific. This is why various climate studies consistently conclude that winter Pacific indices provide the optimum predictive potential for boreal spring rainfall in Brazil.

The fact that we see only a very weak SSTA connection in the western equatorial Atlantic, in spite of ENSO-related zonal wind anomalies there, may be due to the opposing effects of buoyancy flux and advection over most of this area. However, one remaining conundrum is the lack of any dynamically produced, remote SST response in the Gulf of Guinea, associated with P_1 (Figure 5). This is confirmed by both our calculations (Figure 5) and by *Zebiak* [1993]. Regardless of the local thermodynamic effects, sustained zonal wind changes along the equator are expected to induce changes in the slope of the equatorial thermocline and consequent cooling or warming in the east (i.e., through changes in thermocline depth and turbulent entrainment). *Zebiak* [1993] found correlations (without regard to the Pacific ENSO) between his ATL3 index of central equatorial Atlantic SSTA (3°S - 3°N ; 0° - 20°W) and western Atlantic zonal wind anomalies that confirm this relationship. Those correlations are consistent with his corresponding modeling results for near-equatorial interactions (i.e., without regard to the Pacific). To quantify this, we calculate a correlation of +0.28 between the ATL3 index and the zonal wind anomalies averaged over 4°S - 2°N , 20°W - 40°W , significant at the 95% level. Hence the amount of SSTA variance normally explained through this relationship is typically small, and when ATL3 is compared with the Pacific ENSO variability, the explained variance disappears entirely. These conclusions are not changed by using an Atlantic SSTA index positioned farther

east nor by limiting the time period to the first or second half of the 43-year temporal domain.

The modeling study by *Latif and Barnett* [1995] suggests that Pacific SSTA does indeed influence the eastern equatorial Atlantic. However, although the response produced is the one expected dynamically as discussed above, it is also one that neither we nor *Zebiak* [1993] have found. *Latif and Barnett* [1995] explain, however, that their results may overemphasize the role of ENSO forcing in the Atlantic. In the case of the Gulf of Guinea, this seems to be the case. In response to the results of *Zebiak* [1993], *Latif and Barnett* [1995] suggest that mismatches in the time periods considered or the SSTA index longitudes used may explain the discrepancy. In particular, their results may have been disproportionately influenced by the very strong 1984 event in the equatorial Atlantic, following the strong 1982-1983 ENSO warming in the Pacific (M. Latif, personal communication, 1995). However, our results, which span the domains of both those studies, indicate that this is not the case. In contrast, where our study finds an important connection to the Pacific (the NE trades region of the tropical North Atlantic), *Latif and Barnett* [1995] find none. However, this is consistent with the fact that their model interactions do not permit a realistic forcing of the ocean mixed layer by thermodynamic surface fluxes, in the way that our study finds to be important (M. Latif, personal communication, 1995).

As a final note, the lack of statistical evidence for linkage between the Pacific ENSO and the Gulf of Guinea should not be interpreted to mean that such linkages cannot occur on a case-by-case basis. It has been rather convincingly shown, for example, that the strong 1984 warming in the eastern equatorial Atlantic was probably the direct result of equatorial zonal wind anomalies forced by the severe 1982-1983 ENSO event in the Pacific [*Delecluse et al.*, 1994; *Carton and Huang*, 1994].

6.3. Consequences for Climatic Teleconnections

This study has identified and explained two regions (NE trades and ITCZ) where changes in the surface winds induced by Pacific ENSO variability result in lag-correlated departures of Atlantic SST. This immediately raises the possibility that some of the observed correlations of land-based climate data with ENSO indices [e.g., *Ropelewski and Halpert*, 1987] may be more directly due to Atlantic SST variations and less so to the Pacific. The best examples of where this may be true are NE Brazil and NW Africa, both of which are close to and influenced by the Atlantic ITCZ. A number of studies have shown that the correlation of NE Brazil rainfall with Atlantic SSTA is stronger than with Pacific indices [e.g., *Hastenrath et al.*, 1984; *Hastenrath and Greischar*, 1993]. Because variability in the regions near the ITCZ appears sensitive to both the ITCZ variability and to the meridional SST gradient [*Moura and Shukla*, 1981; *Folland et al.*, 1986] and since the Pacific ENSO influences both of these factors, it appears quite plausible that apparent ENSO connections to the land climate are primarily reflections of the relationships linking Atlantic SSTA and ITCZ behavior to the Pacific. The intercorrelation between Atlantic and Pacific SST predictors is reason to exercise caution in the interpretation of western hemisphere climatic teleconnections with respect to either ocean alone.

7. Conclusions

The principal conclusions from this study are:

1. The large-scale variability of tropical Atlantic SSTA is well represented by two dominant EOF modes that summarize independent fluctuations in tropical regions south and north of

the ITCZ. At the mostly interannual timescales examined here, meridionally antisymmetric behavior is not a dominant characteristic of Atlantic SSTA variability. Dipole configurations do occur randomly, however, and there is a weak tendency for a small region west of Angola to be anticorrelated with the North Atlantic during the boreal late winter and early spring.

2. The Pacific ENSO variability is strongly correlated with SSTA in the tropical North Atlantic along 10°-20°N, and also (but somewhat less so) just north of the ITCZ and in the western South Atlantic along a 20°-25°S band. Statistically, the ENSO-related Atlantic fluctuations lag their Pacific counterparts by 4-5 months. The primary ENSO pattern in the tropical North Atlantic is most intense and areally extensive in the boreal spring (April-May-June), while the South Atlantic pattern is best developed in the boreal summer (June-July-August).

3. To first order, the ENSO response pattern is not antisymmetric, with the South Atlantic dominated more by positive correlations than negative ones, that is, of the same sign as the stronger correlations in the North Atlantic. However, there is a tendency for weak negative correlations to occur in the eastern low-latitude South Atlantic off the Angolan coast during the late spring and early summer.

4. The principal region of ENSO connectivity under the NE trades is forced by changes in surface wind speeds that are in turn associated with tropospheric changes induced by equatorial Pacific warmings. The wind speed changes affect the mixed layer temperature primarily through evaporation, entrainment, and sensible heat transfer, in decreasing order of importance.

5. The region of secondary covariability with ENSO, occurring along the northern edge of the mean ITCZ position, appears to be associated with northward migrations of the ITCZ that are influenced by the North Atlantic ENSO-related warmings and southward migrations of the ITCZ that are influenced by the North Atlantic ENSO-related coolings.

6. The intercorrelation between Atlantic and Pacific SST predictors of land climate is reason to exercise caution in the interpretation of western hemisphere climatic teleconnections with respect to either ocean alone.

Acknowledgments. This work has greatly benefited from discussions with colleagues, including G. Halliwell, R. Houghton, Y. Tourre, M. Latif, S. Zebiak, and V. Mehta. We are grateful for the constructive comments of an anonymous reviewer who encouraged us to expand on our analysis of the seasonal evolution of the relationships. We thank R. Reynolds for sharing the *Smith et al.* [1996] data set with us prior to the publication of their paper. The research has been supported by the Pan-American Climate Studies (PACS; GC95-807) program, the Inter-American Institute for Global Change Research through the University Corporation for Atmospheric Research (IAI/UCAR; S-9681694), and the Environmental Research Laboratories (ERL) of the National Oceanic and Atmospheric Administration.

References

- Barnston, A., et al., Long-lead seasonal forecasts — Where do we stand? *Bull. Am Meteorol. Soc.*, 75, 2097-2114, 1994.
- Bjerknes, J., Atlantic air-sea interaction, *Adv Geophys.*, 10, 1-82, 1964.
- Cardone, V.J., J.G. Greenwood, and M. A. Cane, On trends in historical marine wind data, *J. Clim.*, 3, 113-127, 1990.
- Carton, J., and B. Huang, Warm events in the tropical Atlantic, *J. Phys. Oceanogr.*, 24, 888-903, 1994.
- Covey, D.C., and S. Hastenrath, The Pacific El Niño phenomenon and the Atlantic circulation, *Mon. Weather Rev.*, 106, 1280-1287, 1978.
- Delecluse, P., C. Levy, K. Arpe, and L. Bengtsson, On the connection between the 1984 Atlantic warm event and the 1982-1983 ENSO, *Tellus, Ser. A*, 46, 448-464, 1994.

- Donoso, M.C., J.E. Harris, and D. B. Enfield, Upper ocean thermal structure of the eastern tropical Pacific, *DOC/NOAA Tech. Rep ERL 450-AOML 36*, 221 pp., National Oceanic and Atmos. Admin., Silver Spring, Md., 1994.
- Esbensen, S.K. and V. Kushnir, *The heat budget of the global ocean: An atlas based on estimates from marine surface observations*, Clim. Res. Inst., Rep. 29, 27 pp., 188 figures, Oreg. State Univ., Corvallis, 1981.
- Folland, C.K., T.N. Palmer, and D.E. Parker, Sahel rainfall and worldwide sea temperatures, 1901-85, *Nature*, 320, 602-607, 1986.
- Frankignoul, C., Sea surface temperature anomalies, planetary waves, and air-sea feedback in the middle latitudes, *Rev. Geophys.*, 23, 357-390, 1985.
- Gray, W.M., Atlantic seasonal hurricane frequency, I: El Niño and 30 mb quasi-biennial oscillation influences, *Mon. Weather Rev.*, 112, 1649-1668, 1994.
- Halliwel, G.R., and D.A. Mayer, Frequency response properties of forced climatic SST anomaly variability in the North Atlantic. *J. Clim.*, in press, 1996.
- Hameed, S., K.R. Sperber, and A. Meinster, Teleconnections of the Southern Oscillation in the tropical Atlantic sector in the OSU coupled upper ocean-atmosphere GCM, *J. Clim.*, 6, 487-498, 1993.
- Hastenrath, S., On modes of tropical circulation and climate anomalies, *J. Atmos. Sci.*, 35, 2222-2231, 1978.
- Hastenrath, S., and L. Greischar, Further work on the prediction of northeast Brazil rainfall anomalies, *J. Clim.*, 6, 743-758, 1993.
- Hastenrath, S., M.-C. Wu, and P.-S. Chu, Toward the monitoring and prediction of north-east Brazil droughts. *Q. J. R. Meteorol. Soc.*, 110, 411-425, 1984.
- Hastenrath, S., L.C. de Castro, and P. Aceituno, The Southern Oscillation in the Atlantic sector, *Contrib. Atmos. Phys.*, 60, 447-463, 1987.
- Houghton, R.W., and Y.M. Tourre, Characteristics of low-frequency sea surface temperature fluctuations in the tropical Atlantic, *J. Clim.*, 5, 765-771, 1992.
- Huang, B., J.A. Carton, and J. Shukla, A numerical simulation of the variability in the tropical Atlantic Ocean, 1980-88, *J. Phys. Oceanogr.*, 25, 835-854, 1995.
- Kundu, P.K., Ekman veering observed near the ocean bottom, *J. Phys. Oceanogr.*, 6, 238-242, 1976.
- Latif, M., and T.P. Barnett, Interactions of the tropical oceans, *J. Clim.*, 8, 952-964, 1995.
- Mehta, V.M., and T. Delworth, Decadal variability of the tropical Atlantic Ocean surface temperature in shipboard measurements and in a global ocean-atmosphere model, *J. Clim.*, 8, 172-190, 1995.
- Moura, A.D., and J. Shukla, On the dynamics of droughts in northeast Brazil: Observations, theory and numerical experiments with a general circulation model, *J. Atmos. Sci.*, 38, 2653-2675, 1981.
- North, G.R., T.L. Bell, R.F. Cahalan, and F. J. Moeng, Sampling errors in the estimation of empirical orthogonal functions, *Mon. Weather Rev.*, 110, 699-706, 1982.
- Philander, S.G.H., and R.C. Pacanowski, The oceanic response to cross-equatorial winds (with application to coastal upwelling in low latitudes), *Tellus*, 33, 201-210, 1981.
- Rasmusson, E.M., and T.C. Carpenter, Variations in tropical sea surface temperature and surface wind fields associated with the Southern Oscillation/El Niño, *Mon. Weather Rev.*, 110, 354-384, 1982.
- Ropelewski, C.F., and M.S. Halpert, Global and regional scale precipitation patterns associated with El Niño/Southern Oscillation, *Mon. Weather Rev.*, 110, 1606-1626, 1987.
- Sciremammano, F., Jr., A suggestion for the presentation of correlations and their significance levels, *J. Phys. Oceanogr.*, 9, 1273-1276, 1979.
- Smith, T.M., R.W. Reynolds, R.E. Livezey, and D.C. Stokes, Reconstruction of historical sea surface temperatures using empirical orthogonal functions. *J. Clim.*, 9, 1403-1420, 1996.
- Wallace, J.M., C. Smith, and Q. Jiang, Spatial patterns of atmosphere-ocean interaction in the northern hemisphere winter, *J. Clim.*, 3, 990-998, 1990.
- Weare, B.C., Empirical orthogonal function analysis of Atlantic Ocean surface temperatures, *Q. J. R. Meteorol. Soc.*, 103, 467-478, 1977.
- Woodruff, S.D., R.J. Slutz, R.L. Jenne, and P.M. Steurer, A comprehensive ocean-atmosphere data set, *Bull. Am. Meteorol. Soc.*, 68, 1239-1250, 1987.
- Zebiak, S.E., Air-sea interaction in the equatorial Atlantic region, *J. Clim.*, 6, 1567-1586, 1993.

D. B. Enfield and D. A. Mayer, Atlantic Oceanographic and Meteorological Laboratory, NOAA, 4301 Rickenbacker Causeway, Miami, FL, 33149. (e-mail: enfield@aoml.aoml.gov)

(Received October 30, 1995; revised June 26, 1996; accepted October 15, 1996.)